SLAC-PUB-9506
September 2002

Neutron Energy and Time-of-flight Spectra Behind the Lateral Shield of a High Energy Electron Accelerator Beam Dump, Part I: Measurements *

S. Taniguchi
Japan Synchrotron Radiation Research Institute, Koto 1-1-1, Mikazuki-cho, Sayo-gun, Hyogo, 679-5198, Japan
T. Nakamura, T. Nunomiya, H. Iwase, S. Yonai, M. Sasaki
Tohoku University, Department of Quantum Science and Energy Engineering, Aoba, Aramaki, Aoba-ku, Sendai, 980-8579, Japan
S. H. Rokni, J. C. Liu, K. R. Kase
Stanford Linear Accelerator Center, Stanford University, Stanford, California 94309
S. Roesler
CERN, CH-1211 Geneva 23, Switzerland

Abstract

Neutron energy and time-of-flight spectra were measured behind the lateral shield of the electron beam dump at the Final Focus Test Beam (FFTB) facility at the Stanford Linear Accelerator Center. The neutrons were produced by a 28.7 GeV electron beam hitting the aluminum beam dump of the FFTB which is housed inside a thick steel and concrete shield. The measurements were performed using a NE213 organic liquid scintillator behind different thicknesses of the concrete shield of 274 cm, 335 cm, and 396 cm, respectively. The neutron energy spectra between 6 and 800 MeV were obtained by unfolding the measured pulse height spectrum with the detector response function. The attenuation length of neutrons in concrete was then derived. The spectra of neutron time-of-flight between beam on dump and neutron detection by NE213 were also measured. The corresponding experimental results were simulated with the FLUKA Monte Carlo code. The experimental results show good agreement with the simulated results.

Submitted to Nuclear Instruments and Methods in Physics Research: Section A. Accelerators

*Work supported by Department of Energy contract DE-AC03-76SF00515

Neutron Energy and Time-of-flight Spectra Behind the Lateral Shield of a High Energy Electron Accelerator Beam Dump, Part I: Measurements

S. Taniguchi, [a] T. Nakamura, [b,*] T. Nunomiya, [b] H. Iwase, [b] S. Yonai, [b] M. Sasaki, [b,e] S. H. Rokni, [c] J. C. Liu, [c] K. R. Kase, [c] S. Roesler, [d]

[a] *Japan Synchrotron Radiation Research Institute, Koto 1-1-1, Mikazuki-cho, Sayo-gun, Hyogo, 679-5198, Japan*

[b] *Tohoku University, Department of Quantum Science and Energy Engineering, Aoba, Aramaki, Aoba-ku, Sendai, 980-8579, Japan*

[c] *Stanford Linear Accelerator Center, Stanford, California 94309, U.S.A.*

[d] *CERN, CH-1211 Geneva 23, Switzerland*

[e] *Central Research Institute of Electric Power Industries, Komae Laboratory, Iwato-Kita, 2-11-1, Komae, Tokyo, Japan*

Abstract

Neutron energy and time-of-flight spectra were measured behind the lateral shield of the electron beam dump at the Final Focus Test Beam (FFTB) facility at the Stanford Linear Accelerator Center. The neutrons were produced by a 28.7 GeV electron beam hitting the aluminum beam dump of the FFTB which is housed

inside a thick steel and concrete shield. The measurements were performed using a NE213 organic liquid scintillator behind different thicknesses of the concrete shield of 274 cm, 335 cm, and 396 cm, respectively. The neutron energy spectra between 6 and 800 MeV were obtained by unfolding the measured pulse height spectrum with the detector response function. The attenuation length of neutrons in concrete was then derived. The spectra of neutron time-of-flight between beam on dump and neutron detection by NE213 were also measured. The corresponding experimental results were simulated with the FLUKA Monte Carlo code. The experimental results show good agreement with the simulated results.

Key words: Electron accelerator; Neutron spectrum; Concrete Shielding; Deep penetration; Organic liquid scintillator; TOF spectrum

1 INTRODUCTION

High-energy electron accelerators are widely used for high-energy physics research, synchrotron radiation applications and many other purposes. They produce neutrons through photonuclear reactions of bremsstrahlung photons generated in targets, beam stops, collimators, etc. Information on high-energy neutron spectra initiated by high-energy electrons is indispensable for the radiation safety and shielding design at high-energy electron accelerator facilities due to the strong penetrability of high-energy neutrons. There are a few recent publications reporting neutron spectra behind thick shields for high-energy proton accelerators [1–3]. However, to our knowledge only one experimental data set of neutron spectra outside thick shields at a high-energy electron ac-

* Corresponding author: Tel: +81-22-217-7805; Fax: +81-22-217-7908

E-mail address: nakamura@cyric.tohoku.ac.jp (T.Nakamura)

celerator [4] has so far been published, and these are reported as preliminary results.

In this study the high-energy neutron spectra between 6 and 800 MeV behind the lateral shield of a 28.7 GeV electron beam dump were measured at the Final Focus Test Beam (FFTB) facility [5] at the Stanford Linear Accelerator Center (SLAC). The measurements were performed using a NE213 organic liquid scintillator behind thick concrete shields that were placed outside the fixed steel and concrete shield of the FFTB housing. The NE213 detector has a much better energy resolution than a conventional Bonner sphere spectrometer which allows the energy spectra to be determined more accurately and with less dependence on the initial guess during the spectrum unfolding process. The neutron energy spectra and time-of-flight (TOF) spectra were obtained by unfolding the measured pulse height data, and by using the start signals from the muon scintillator placed down beam of the dump, respectively. The experimental results were also simulated with the FLUKA Monte Carlo code [6,7]. Details of the simulations are described elsewhere [8].

2 EXPERIMENT

The measurements were performed during the period from June 14 to June 23, 2001 using the 28.7 GeV electron beam at the FFTB facility that was extracted from the SLAC linear accelerator at repetition rates of 10 to 30 Hz. The number of electrons in each beam pulse was monitored with a Toroid Charge Monitor (TCM). The beam intensity was varied from 2×10^9 to 5×10^9 electrons/pulse in order to minimize pulse pile-up in the detector. Figure 1 shows the schematic layout in the vertical plane of the FFTB facility.

Figure 2 shows horizontal and vertical cross-sectional views of the FFTB dump together with the locations of the NE213 detector and the muon counter used in this study. Figure 3 is the schematic view of the experimental setup. The aluminum beam dump of 145 cm length and 38 cm diameter stops fully the electron beam. The dump is placed in a room shielded laterally by 84 cm of steel and that is surrounded with a 183 cm thick concrete wall. Blocks of steel are placed outside the room in the forward direction to the beam line to attenuate muons generated in the dump.

To measure the energy and time-of-flight spectra of neutrons produced in the beam dump, a NE213 detector of 12.7 cm diameter and 12.7 cm thickness was placed about 36 cm from the concrete floor in a hutch at 90 degrees with respect to the beam direction behind the steel and concrete shield walls. The detector is coupled with a R4144 photomultiplier connected to an E1458 base (Hamamatsu Photonics Co. Ltd.), which is designed to expand the dynamic range of output pulses for high-energy neutron measurements [9]. The muon scintillator, which is a 0.625 cm thick by 10.16×30.48 cm^2 plastic scintillator coupled with a RCM8575 photomultiplier, was set in the muon shield at 335 cm distance to the outer shield surface in order to use it as the event trigger and for start signals of the TOF measurements. The measurements were performed with added concrete shielding of three different thicknesses of 91, 152, and 213 cm between the fixed wall and the detector. Thus, the total thicknesses of concrete shield are 274, 335, and 396 cm, respectively. The results can be used to investigate the attenuation profile and the equilibrium spectra. Table 1 shows for each shield thickness, the beam intensity and total electron numbers incident on the beam dump during each measurement. Table 1 also gives the total counts above the threshold (set at 3 MeVee as described below)

per beam pulse, the fractions of pile-up events and neutron events relative to total events, expressed as percent. The fraction of pile-up events is rather large, 24 % for the 91- cm thick added concrete, and decreases with increasing shield thickness. Thus, a correction for pile-up events is necessary and was made as described later.

Figure 4 shows the electronic circuit, which is simplified from the actual electronic circuit for clarity. The output signal of the muon scintillator was used as the event trigger and as the start signal of time-to-digital converter (TDC) for TOF. The integrated charges of the "total" and "slow" (decay) components of the signals from the NE213 detector were measured by the charge analog-to-digital converter (QDC) to distinguish between neutrons and gamma rays, the so-called neutron-gamma pulse-shape discrimination. To obtain the total and slow light output pulse components, the total gate width was set at 200 ns during which the entire signal is integrated. The slow gate start is delayed 30 ns from the peak of the output signal and the width is also 200 ns. The output pulses from the NE213 were also used as stop signals of the TDC for TOF. The time difference between the pulses of the muon scintillator and the NE213 detector, which represents the difference between the beam-on-dump time and the particle detection time , was also measured for comparison with the simulation with the FLUKA Monte Carlo code [8]. All of these processes were controlled by the KODAQ data-acquisition system (Kakuken Online Data Acquisition System) [10].

The linearity of the TCM was checked with a special calibration module at various times during the experiment. Figure 5 shows the excellent linearity of the TCM as an electron beam monitor.

3 DATA ANALYSIS

The neutron events were separated from the gamma-ray events by using two-dimensional graphical plots of total and slow pulse components of the NE213 detector as shown in Fig. 6a. Pile-up events were also eliminated using Fig. 6a. Fig. 6b shows the cross-sectional view of slow pulse components at two total pulse heights, A and B, which allows clear identification and discrimination of the gamma-ray and neutron events. The fraction of pile-up events is larger for thinner (91 cm thick) additional concrete shield, because of higher counting rates, as shown in Table 1. The fraction of neutron events does not change much with changing shield thickness as seen in Table 1. As a first approximation, all the pile-up events were assumed to consist of two pulses (neutron-neutron, neutron-photon, or photon-photon). Thus, the absolute values of neutron pulse counts were multiplied simply by the following pile-up correction factor, F:

$$F = (Nn + Ng + 2Np)/(Nn + Ng) \tag{1}$$

where Nn, Ng, and Np are the counts of neutron, gamma-ray, and pile-up events. The F values obtained are shown in Table 1. For 91 cm thick added concrete, the pile-up correction factor of 1.64 is quite large.

When charged particles produced by neutron interactions in the scintillator (mainly recoil protons by the H(n,n)p elastic collision) escape from the NE213 detector without complete energy loss, the pulse shapes of high-energy neutron events become close to those of gamma-ray events, the so-called "wall effect". Since it is not possible to discriminate between the gamma-ray events and the escaping charged particle events, both types of events were removed from

the neutron events. Therefore, the response functions of the NE213 detector must also exclude the light outputs caused by escaping charged particles, which have been determined experimentally in the neutron energy range from 6 MeV (corresponding to 3 MeVee, as given in Ref. [9]) to 800 MeV by Sasaki et al. [12].

The light output data in each channel are converted into the light output unit of MeVee by using the Compton edges in the spectra of a ^{60}Co gamma-ray source (1.17 and 1.33 MeV, average of 1.25 MeV) and an ^{241}Am-Be source (4.43 MeV). The ^{60}Co bias was determined with a channel having 0.303 times the counts of the Compton edge due to a 1.25 MeV gamma ray, which corresponds to 1.15 MeVee. For the calibration for higher light output, Eq. (3) of Ref. [9] was used.

The neutron energy spectrum was obtained with the unfolding technique using the FORIST code [13] and response functions for neutrons from 6 to 800 MeV [12]. In the analysis the threshold of the light output pulses was set to 3 MeVee corresponding to the threshold of the response function. In addition, the window function in the FORIST code was adjusted to obtain a reasonable convergence by varying the energy resolution valuesbetween 10 % and 200 %.

4 RESULTS AND DISCUSSION

4.1 TOF Spectra

Figure 7 shows the pile-up corrected experimental neutron TOF spectra (points) in cps units behind the three different total shield thicknesses of 274, 335,

and 396 cm, respectively, in comparison with the results calculated with the FLUKA code [8] (histograms). When FLUKA-calculated neutron currents above 6 MeV (3 MeVee) are folded with the detection efficiency of the NE213 detector as a function of neutron energy, the calculated TOF spectra can be directly compared with the measured count rates as a function of time-of-flight in nano-seconds. The detection efficiency, having a light output threshold of 3 MeVee, is given by the Cecil code [14], which is accurate to within 10 to 15 % up to the neutron energy of several hundreds of MeV [15]. Note that, in this experiment, the absolute time reference for TOF was not established. Therefore, the measured TOF spectra were arbitrarily shifted to match the peaks of the calculated TOF spectra. The agreement in the shapes of TOF spectra between experiment and calculation is acceptable, especially for the 274 cm thickness,. The longer tails for larger TOFs in the measured distributions could be due to the time resolution of the measuring circuit. The measured TOF spectrum for the 335 cm shield shows a small peak at very low TOF that is not seen in the calculation. This spurious peak might come from a small contribution to the neutron events that are produced by beam loss on a collimator (see Fig. 1), which is located upstream of the FFTB beam dump.

4.2 Energy Spectra

Figure 8 gives the light output distribution of total pulse components for events without pile-up correction for the three different concrete shield thicknesses. The solid lines are total events before neutron-photon discrimination, and the dots are only neutron events above 3 MeVee threshold. In Fig. 9 the neutron energy spectra unfolded with the FORIST code (points) are compared with

the spectra calculated with the FLUKA code [8] (histograms). The upper and lower graphs give the measured spectra per MeV and per lethargy both after pile-up correction for one electron incident on the beam dump measured with the TCM, respectively. The measured spectra after pile-up correction generally give good agreement with the calculated spectra both in spectral shapes and in absolute values in the energy region from 6 MeV to 200 MeV. In the energy region above 200 MeV the measured energy spectra are lower than the calculated spectra. This could be in part due to very poor statistics of detected counts and also due to the poor accuracy of the response function of the NE213 detector [12] caused by low neutron detection efficiency in the high-energy region. For the 274 cm shield, the pile-up corrected measured spectrum gives a somewhat smaller value than the calculated spectrum in the energy region around 20 MeV. This underestimation may partly come from the larger contribution of the pile-up events, which could not be completely corrected as described before.

4.3 Attenuation Profiles of Neutron Flux and Ambient Dose Equivalent

From the energy spectra shown in Fig. 9 the total neutron fluences integrated between 6 MeV and 800 MeV for the measured (unfolded) energy spectra and between 6 MeV and 885 MeV for the calculated spectra were obtained. Table 2 shows the comparison between experimental (E) and calculated total fluences (C) together with the ratios of the two values. The measured fluence result for 274 cm thick concrete is 30 % lower than the calculated result due to the relatively large fraction of pile-up events, but for 335 and 396 cm thick concrete, the agreement between experiment and calculation is excellent.

The measured and calculated ambient dose equivalents above 6 MeV were obtained by multiplying the pile-up corrected energy spectra and the calculated spectra with the fluence-to-ambient dose equivalent conversion factor given in ICRP Publ. 74 [16] up to 200 MeV. At higher energies a constant value (the value for 200 MeV) is assumed. These results are also shown in Table 2. Similar a the total fluence, the measured dose equivalent result for 274 cm thick concrete is 34 % lower than the calculated result. However, for 335 and 396 cm thick concrete, the agreement between experiment and calculation is again very good. The measured and calculated ambient dose equivalents multiplied by the square of the distance between the center of the dump and the detector are shown in Fig. 10 as a function of total concrete shield thickness in g/cm^2 (concrete density of 2.35 g/cm^3). Also shown in Fig. 10 is a transmission curve calculated with the widely used analytical formula given by Jenkins [17].

The measured and FLUKA-calculated attenuation lengths λ_ϕ(g/cm2) of neutron fluences above 6 MeV and λ_D(g/cm2) of neutron ambient dose equivalents above 6 MeV in concrete were obtained by a least squares fit to the three measured data points shown in Table 2 and Fig. 10 (fluences and ambient dose equivalents multiplied by the square of the distance between the center of the dump and the detector). The λ_ϕ and λ_D values are given in Table 3 together with their respective standard deviations. As expected for equilibrium spectra both measured and calculated values of λ_ϕ and λ_D are all in good agreement and are also close to the value of 120 g/cm^2 for high energy neutrons used in the Jenkins' formula.

5 CONCLUSION

Neutron energy and time-of-flight spectra behind thick concrete shielding at 90 degrees to the 28.7 GeV electron beam dump of the FFTB facility at SLAC were measured in the energy range from 6 MeV to 800 MeV by using a NE213 organic liquid scintillator. The measurements were performed at three different concrete shield thicknesses of 274 cm, 335 cm, and 396 cm, respectively.

The spectra were also compared with simulations performed with the FLUKA Monte Carlo particle transport code. The measured neutron spectra show good agreement with the calculated spectra, especially for the 335 cm and 396 cm concrete shield thicknesses. Measured and calculated values for attenuation length are also in good agreement. The measured and calculated neutron TOF spectra were also compared. This provides an unique and efficient benchmark that avoids the ambiguities of unfolding techniques that are present in comparisons of energy spectra. These experimental data will be a good benchmark for deep penetration of high-energy neutrons through a concrete shield for high-energy electron accelerator facilities and for checking the accuracy of transport codes and analytical formulas used in shielding design.

ACKNOWLEDGMENTS

The authors are grateful to Clive Field, Ronald Seefred, and the staff of Accelerator Operation and the Experimental Facility Department at SLAC for their support and assistance in setting up the experiment, and operation of the electron beam. This work was supported in parts by the U.S. Department of Energy under contract DE-AC03-76SF00515.

References

[1] G.R.Stevenson, K.L.Liu, R.H.Thomas, Health Phys. 43 (1982) 13.

[2] S.Ban, H.Hirayama, K.Katoh, Nucl. Instr. and Meth. 184 (1981) 409.

[3] T.Nunomiya, N.Nakao, P.Wright, T.Nakamura, E.Kim, T.Kurosawa, S.Taniguchi, M.Sasaki, H.Iwase, Y.Uwamino, T.Shibata, S.Ito, D.R.Perry, Nucl. Instr. and Meth. B 179 (2001) 89.

[4] V.Vylet, J.C.Liu, S.H.Rokni, L.X.Thai, Rad. Protect. Dosim. 70 (1997) 425.

[5] S.H. Rokni, E.C. Benson, D.L. Burke, T.M. Jenkins, J.C. Liu, G. Nelson, W.R. Nelson, H.E. Smith, P. Tenenbaum, D.R. Walz, V. Vylet, Health Phys.71 (1996) 786.

[6] A. Fasso, A. Ferrari, P. R. Sala, "Electron-photon transport in FLUKA: status," Proceedings of the International Conference on Advanced Monte Carlo for Radiation Physics, Particle Transport Simulation and Applications, Monte Carlo 2000, Lisbon, Portugal, October 23-26, 2000, p. 159, A. Kling, F. Barao, M. Nakagawa, L. Tavora, and P. Vaz (Eds.), Springer-Verlag Berlin Heidelberg, (2001).

[7] A. Fasso, A. Ferrari, J. Ranft, P. R. Sala, "FLUKA: Status and perspectives for hadronic applications," Proceedings of the International Conference on Advanced Monte Carlo for Radiation Physics, Particle Transport Simulation and Applications, Monte Carlo 2000, Lisbon, Portugal, October 23-26, 2000, p. 955, A. Kling, F. Barao, M. Nakagawa, L. Tavora, and P. Vaz (Eds.), Springer-Verlag Berlin Heidelberg, (2001).

[8] S.Roesler, J.C.Liu, S.H.Rokni, S.Taniguchi, "Neutron energy and time-of-flight spectra behind the lateral shield of a high energy electron accelerator beam dump, Part II: Monte Carlo simulations" , in preparation.

[9] N.Nakao, T.Nakamura, M.Baba, Y.Uwamino, N.Nakanishi, H.Nakashima, S.Tanaka, Nucl. Instr. and Meth. A 362 (1995) 454.

[10] K.Omata, Y.Fujita, N.Yoshikawa, M.Sekiguchi, Y.Shida, "A data acquisition system based on a personal computer", INS-Rep. 884, Institute for Nuclear Study, University of Tokyo, 1991.

[11] N. Nakao, Y. Uwamiro, T. Nakamura, T. Shibata, N. Nakarishi, M. Takada, E. Kim, T. Kurosawa, Nucl. Instr. and Meth., A 420 (1999) 218.

[12] M.Sasaki, N.Nakao, T.Nakamura, T.Shibata, A.Fukumura, Nucl. Instr. and Meth. A 480 (2002) 440.

[13] R.H.Johnson, B.W.Wehring, ORNL/RSIC-40, Oak Ridge National Laboratory (1976).

[14] R.A.Cecil, B.D.Anderson, R.Madey, Nucl. Instr. and Meth. 161 (1979) 439.

[15] N.Nakao, T.Kurosawa, T.Nakamura, Y.Uwamino, Nucl. Instr. and Meth. A 476 (2002) 176.

[16] International Commission on Radiation Protection, "Conversion Coefficients for Use in Radiological Protection against External Radiation", ICRP Publ. 74 (1995).

[17] T.M.Jenkins, Nucl. Instr. and Meth. 159 (1979) 265.

Captions of figures and tables

Figure 1. Schematic view (elevation) of the FFTB beam line at SLAC.

Figure 2. Horizontal and vertical cross-sectional views of the FFTB dump. The locations of the NE213 detector and muon counter are also shown.

Figure 3. Schematic view of the experimental setup.

Figure 4. Simplified block diagram of the electronic circuit for the measurement using a NE213 scintillator; PM: photomultiplier, HV: high voltage power supply, CFD: constant fraction discriminator, COIN: coincidence unit, GG: gate and delay generator, ADC: analog-to-digital converter, QDC: charge analog-to-digital converter, TDC: time-to-digital converter, TCM: toroid charge monitor.

Figure 5. Linearity check of the TCM using the calibration module.

Figure 6. (a) Two-dimensional graphical plots of total vs. slow components of light output pulses of the NE213 detector for neutron and gamma-ray discrimination. (b) Cross-sectional view of slow components at two total pulse heights, A and B, shown in Fig. 6(a).

Figure 7. Measured time-of-flight spectra (points) penetrated through 274, 335, and 396 cm thick concrete shields compared with those calculated with the FLUKA code (histograms). The measured results are given after pile-up correction.

Figure 8. Measured light output distributions of total-component events (curves are neutron plus gamma events; points are neutron events) for 274, 335 and

396 cm thick concrete shields before pile-up correction.

Figure 9. Measured (points) neutron energy spectra penetrated through 274, 335 and 396 cm thick concrete shields compared with those calculated with the FLUKA code (histogram). The upper and lower graphs give the measured results after pile-up correction in units of cm^{-2} MeV^{-1} and cm^{-2} $lethargy^{-1}$ per one electron incident on the beam dump, respectively.

Figure 10. Attenuation profiles of neutron ambient dose equivalent between 6 MeV and 800 MeV in concrete. The measured results after pile-up correction and the calculated results are compared with the analytical formula by Jenkins [17]. R is the distance between the beam axis (center of the dump) and the detector.

Table 1. Measurement conditions for each of the shield thicknesses. Given are the beam intensity, the total electron numbers, the total counts above the threshold (set at 3 MeVee) per pulse, the fractions of neutron and pile-up events, and the pile-up correction factor F.

Table 2. Total neutron fluxes and ambient dose equivalents integrated between 6 MeV to 800 MeV for experimental results and between 6 MeV to 885 MeV for FLUKA-calculated results. In addition the ratios between calculated and measured values are given.

Table 3. Attenuation lengths for neutron fluences and ambient dose equivalents obtained from the pile-up corrected results and from the FLUKA-calculated results.

Table 1

Concrete shield thickness (cm)	Beam intensity (electron/pulse)	Total number of electrons on dump (electron)	Count/pulse (above 3 MeVee threshold, %)	Pile up event fraction (%)	Fraction of neutron events (%)	Pile-up correction factor (F)
274	2×10^9	2.1×10^{15}	9.6	24	59	1.64
335	5×10^9	6.9×10^{15}	11	13	70	1.30
396	5×10^9	1.4×10^{16}	3.1	7	67	1.15

Table 2

Concrete shield thickness [cm]	Fluence [cm^{-2} $electron^{-1}$]	C/E	Dose [pSv $electron^{-1}$]	C/E	Distance - beam dump to detector [m]
274	Cal. 3.59×10^{-12}	1.30	Cal. 1.30×10^{-9}	1.34	5.49
	Exp. 2.77×10^{-12}		Exp. 9.65×10^{-10}		
335	Cal. 9.30×10^{-13}	1.00	Cal. 3.41×10^{-10}	1.02	6.10
	Exp. 9.34×10^{-13}		Exp. 3.33×10^{-10}		
396	Cal. 1.97×10^{-13}	1.08	Cal. 7.09×10^{-11}	1.04	6.71
	Exp. 1.83×10^{-13}		Exp. 6.84×10^{-11}		

Table 3

	Experiment [g cm^{-2}]	Calculation [g cm^{-2}]
Fluence	125 ± 4	123 ± 5
Dose	125 ± 4	124 ± 6

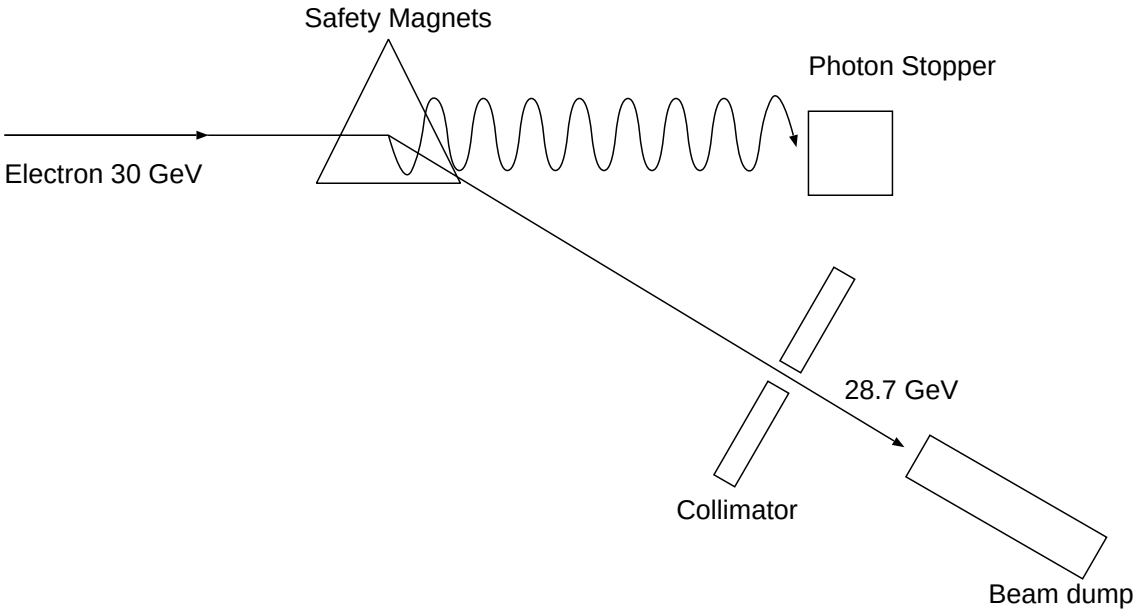
Safety Magnets
Photon Stopper
Electron 30 GeV
28.7 GeV
Collimator
Beam dump

Fig. 1.

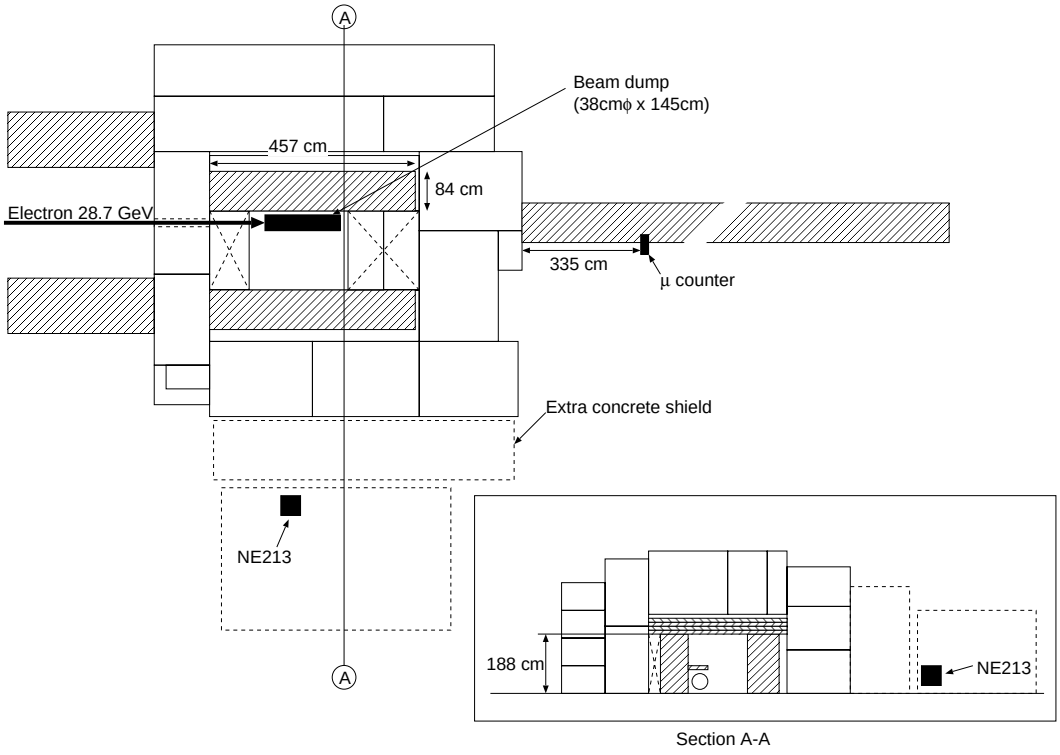
A
Beam dump
(38cmϕ x 145cm)
457 cm
84 cm
Electron 28.7 GeV
335 cm
μ counter
Extra concrete shield
NE213
A
188 cm
NE213
Section A-A

Fig. 2.

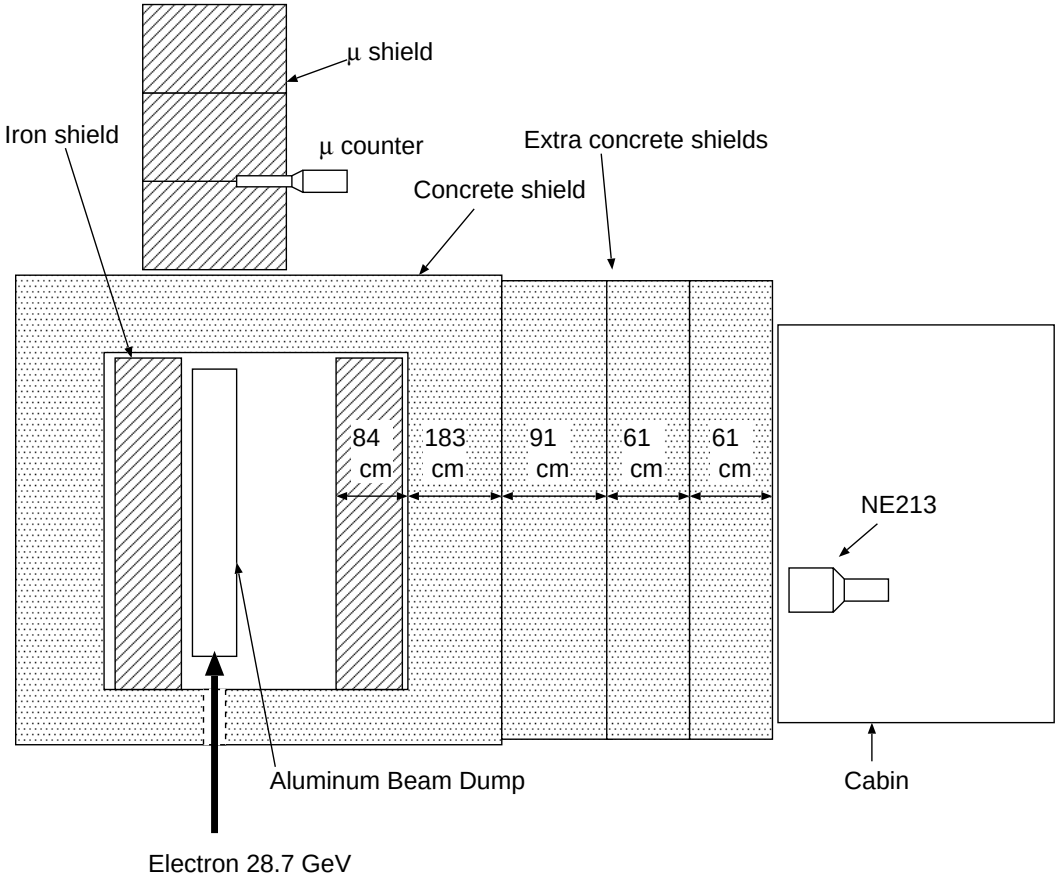
μ shield
Iron shield
μ counter
Extra concrete shields
Concrete shield
84 cm
183 cm
91 cm
61 cm
61 cm
NE213
Aluminum Beam Dump
Cabin
Electron 28.7 GeV

Fig. 3.

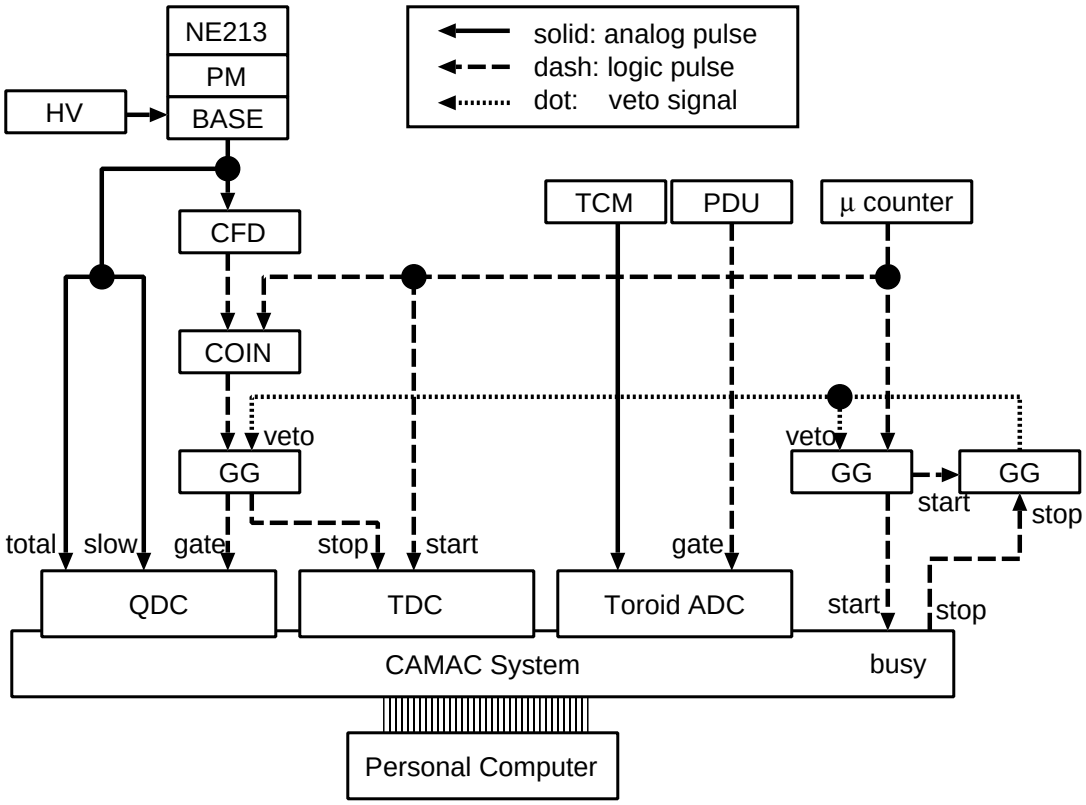
NE213
PM
BASE
HV
solid: analog pulse
dash: logic pulse
dot: veto signal
TCM
PDU
μ counter
CFD
COIN
veto
GG
veto
GG
GG
start
stop
total
slow
gate
stop
start
gate
QDC
TDC
Toroid ADC
start
stop
CAMAC System
busy
Personal Computer

Fig. 4.

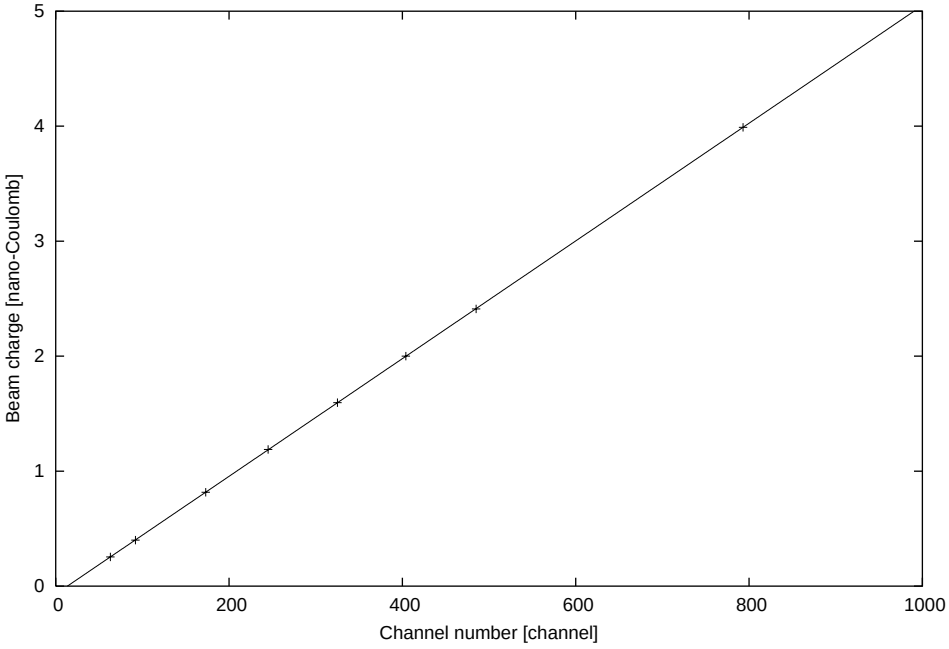
Beam charge [nano-Coulomb]
Channel number [channel]
0
1
2
3
4
5
0
200
400
600
800
1000

Fig. 5.

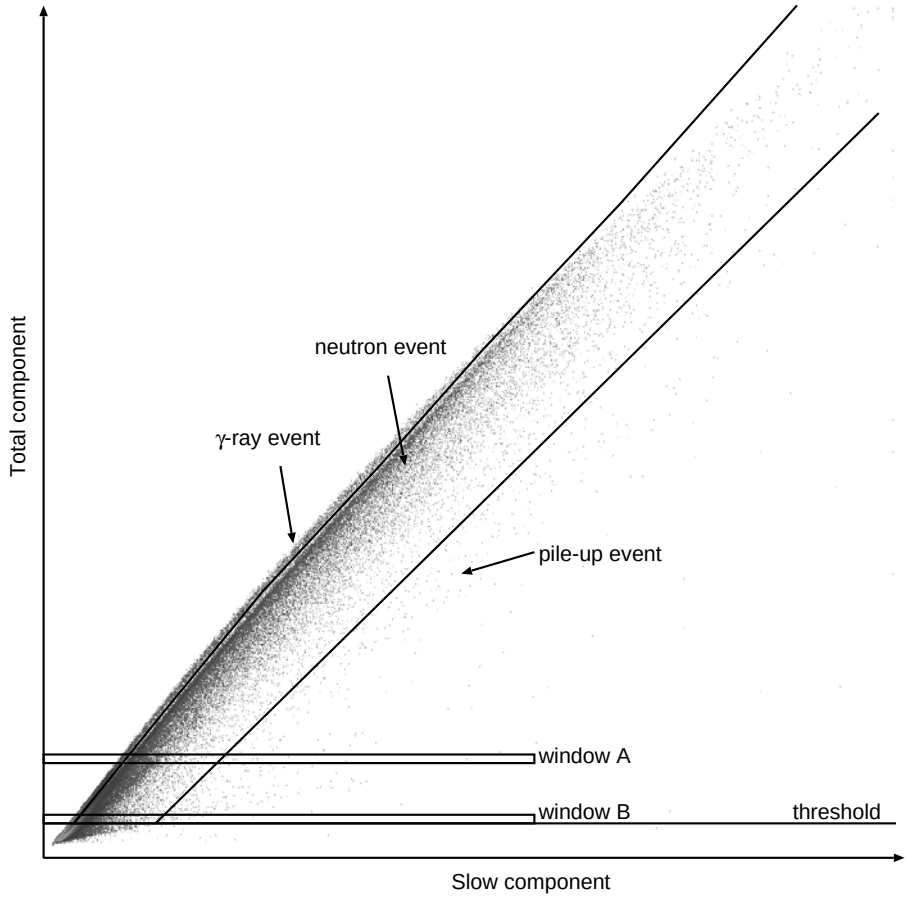
Total component
neutron event
γ-ray event
pile-up event
window A
window B
threshold
Slow component

(a)

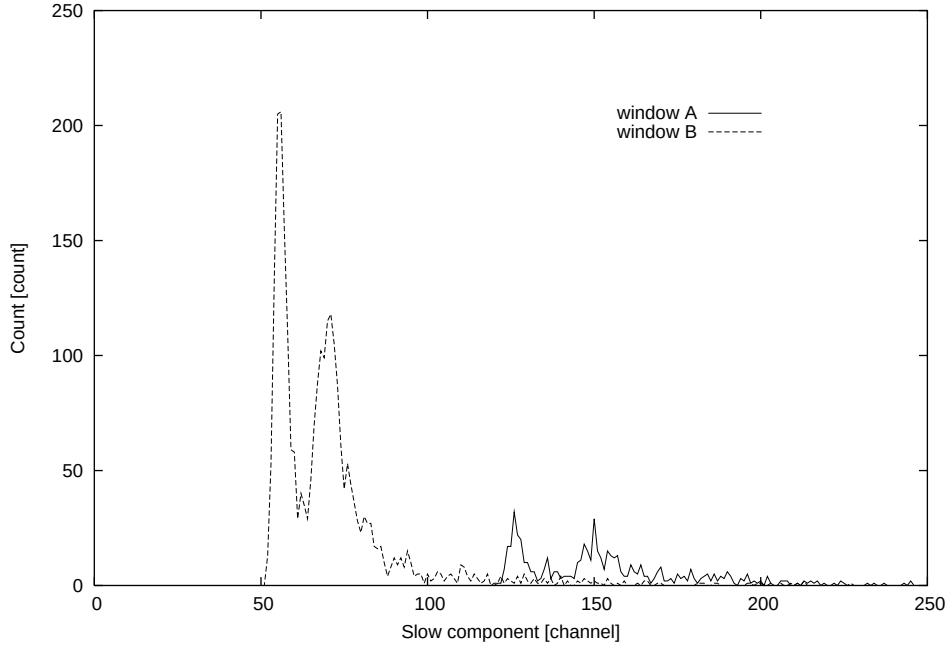
window A
window B
Count [count]
Slow component [channel]
0
50
100
150
200
250

(b)

Fig. 6.

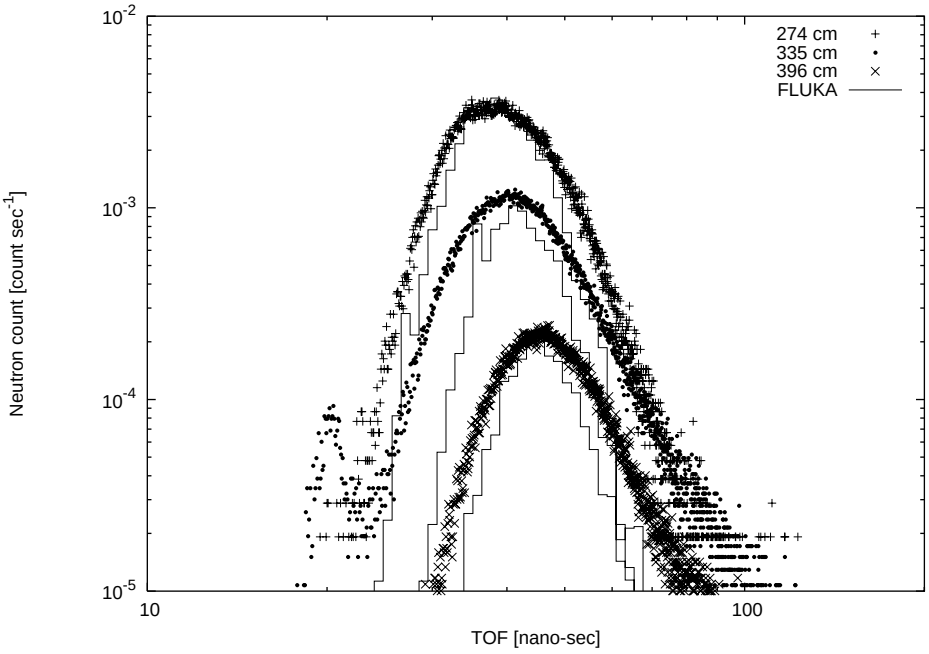
274 cm
335 cm
396 cm
FLUKA
Neutron count [count sec^{-1}]
10^{-2}
10^{-3}
10^{-4}
10^{-5}
10
100
TOF [nano-sec]

Fig. 7.

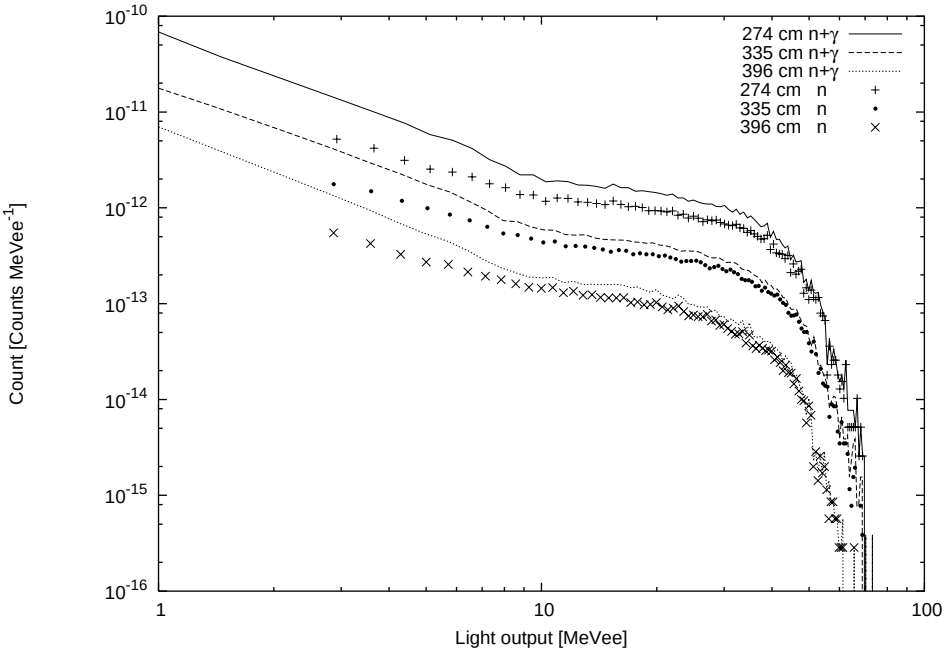
274 cm n+γ
335 cm n+γ
396 cm n+γ
274 cm n
335 cm n
396 cm n
Count [Counts MeVee-1]
Light output [MeVee]
10-10
10-11
10-12
10-13
10-14
10-15
10-16
1
10
100

Fig. 8.

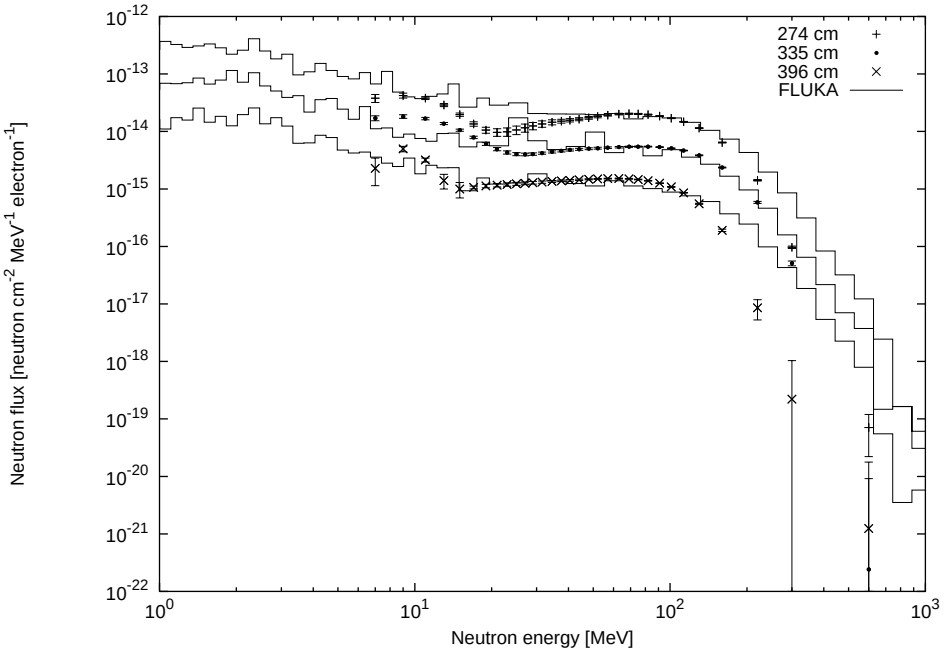
274 cm
335 cm
396 cm
FLUKA
Neutron flux [neutron cm-2 MeV-1 electron-1]
Neutron energy [MeV]

(a)

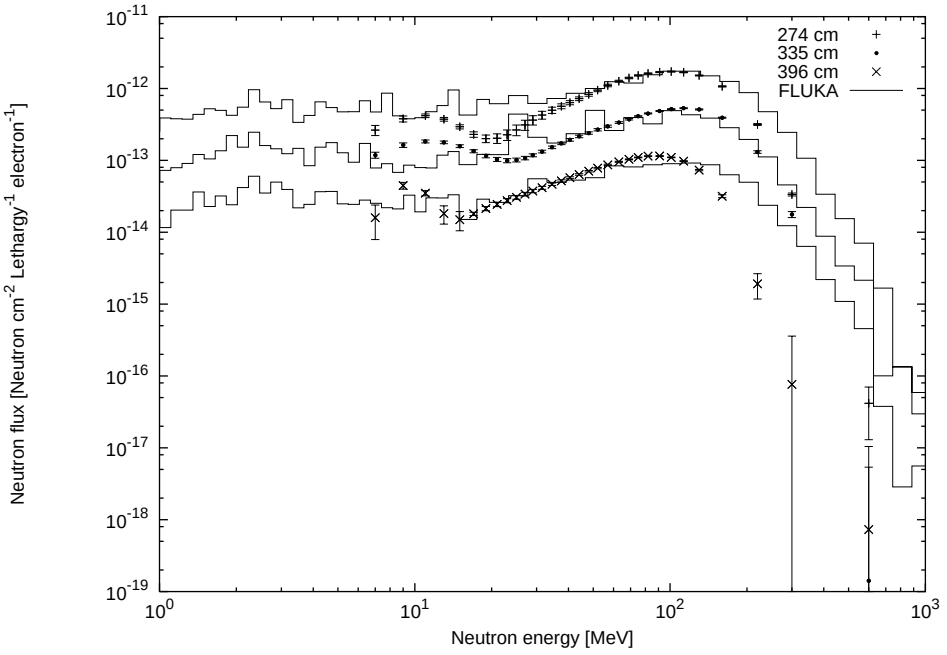
274 cm
335 cm
396 cm
FLUKA
Neutron flux [Neutron cm-2 Lethargy-1 electron-1]
Neutron energy [MeV]

(b)

Fig. 9.

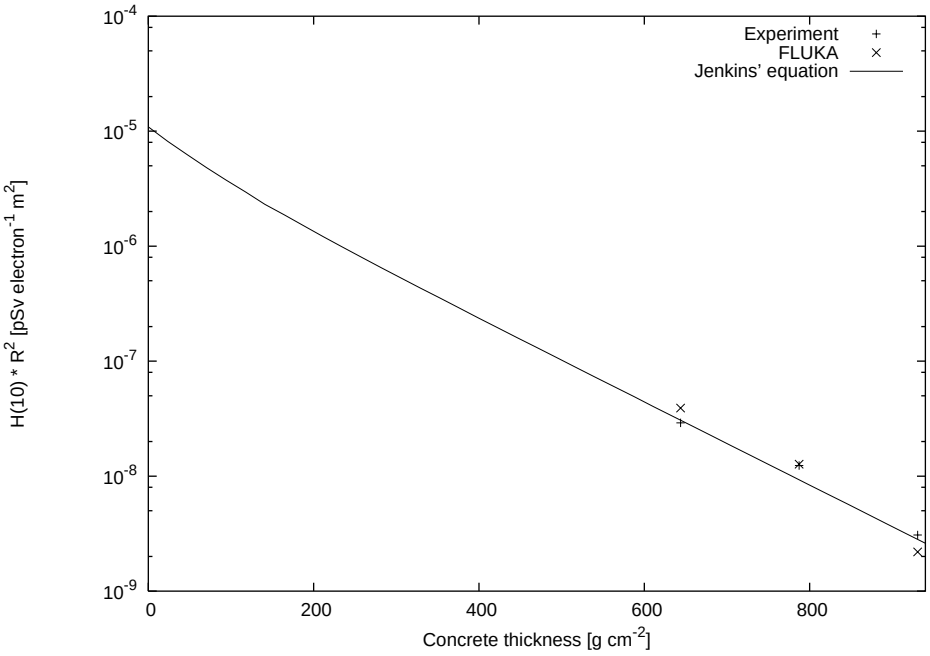
Experiment
FLUKA
Jenkins' equation
H(10) * R^2 [pSv electron^-1 m^2]
Concrete thickness [g cm^-2]
10^-4
10^-5
10^-6
10^-7
10^-8
10^-9
0
200
400
600
800

Fig. 10.